

Titre: On the convergence of stochastic gradient descent in low-precision number formats
Title:

Auteurs: Matteo Cacciola, Antonio Frangioni, Masoud Asgharian, Alireza Ghaffari, & Vahid Partovi Nia
Authors:

Date: 2023

Type: Communication de conférence / Conference or Workshop Item

Référence: Cacciola, M., Frangioni, A., Asgharian, M., Ghaffari, A., & Nia, V. P. (février 2023). On the convergence of stochastic gradient descent in low-precision number formats [Communication écrite]. 12th International Conference on Pattern Recognition Applications and Methods (ICPRAM 2023), Lisbon, Portugal.
Citation: <https://doi.org/10.5220/0011795500003411>

 **Document en libre accès dans PolyPublie**
Open Access document in PolyPublie

URL de PolyPublie: <https://publications.polymtl.ca/54349/>
PolyPublie URL:

Version: Version officielle de l'éditeur / Published version
Révisé par les pairs / Refereed

Conditions d'utilisation: CC BY-NC-ND
Terms of Use:

 **Document publié chez l'éditeur officiel**
Document issued by the official publisher

Nom de la conférence: 12th International Conference on Pattern Recognition Applications and Methods (ICPRAM 2023)
Conference Name:

Date et lieu: 2023-02-22 - 2023-02-24, Lisbon, Portugal
Date and Location:

Maison d'édition: SciTePress
Publisher:

URL officiel: <https://doi.org/10.5220/0011795500003411>
Official URL:

Mention légale: CC BY-NC-ND 4.0
Legal notice:

On the Convergence of Stochastic Gradient Descent in Low-Precision Number Formats

Matteo Cacciola^{1,2}^a, Antonio Frangioni³^b, Masoud Asgharian⁴^c, Alireza Ghaffari¹^d
and Vahid Partovi Nia¹^e

¹*Huawei Noah's Ark Lab, Montreal Research Centre, 7101 Park Avenue, Montreal, Quebec H3N 1X9, Canada*

²*Polytechnique Montreal, 2900 Edouard Montpetit Blvd, Montreal, Quebec H3T 1J4, Canada*

³*Dipartimento di Informatica, Università di Pisa, Largo B. Pontecorvo 3, Pisa, 56127, Italy*

⁴*Department of Mathematics and Statistics, McGill University, 805 Sherbrooke Street West, Montreal, H3A 0B9, Quebec, Canada*

Keywords: Convergence Analysis, Floating Point Arithmetic, Low-Precision Number Format, Optimization, Quasi-Convex Function, Stochastic Gradient Descent.

Abstract: Deep learning models are dominating almost all artificial intelligence tasks such as vision, text, and speech processing. Stochastic Gradient Descent (SGD) is the main tool for training such models, where the computations are usually performed in single-precision floating-point number format. The convergence of single-precision SGD is normally aligned with the theoretical results of real numbers since they exhibit negligible error. However, the numerical error increases when the computations are performed in low-precision number formats. This provides compelling reasons to study the SGD convergence adapted for low-precision computations. We present both deterministic and stochastic analysis of the SGD algorithm, obtaining bounds that show the effect of number format. Such bounds can provide guidelines as to how SGD convergence is affected when constraints render the possibility of performing high-precision computations remote.

1 INTRODUCTION

The success of deep learning models in different machine learning tasks have made these models de facto for almost all vision, text, and speech processing tasks. Figure 1 depicts the size of deep learning models, indicating an exponential increase in the size of the models, and hence an urge for efficient computations. A common technique used in training deep learning models is SGD but the theoretical behaviour of SGD is rarely studied in low-precision number formats. Although there is a surge of articles on real numbers (for example see (Polyak, 1967), (Schmidt et al., 2011), (Ram et al., 2009)), the performance of SGD in low-precision number formats started recently. Depending on the precision, the loss landscape can change considerably. Figure 2, for instance,

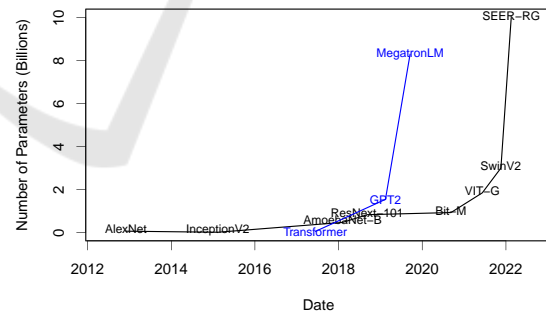




Figure 1: Exploding trend of deep models for image classification (black) and language models (blue) in time.


depicts this situation for ResNet-18 loss landscape in both single-precision and low-precision number formats. Motivated by Figure 2, we present a formal study of SGD for quasi-convex functions when computations are performed in low-precision number formats.


We note that numerical errors, both in forward and back propagation, can possibly affect the convergence behaviour of the algorithm. It is conceivable that the numerical errors should increase as the pre-

^a <https://orcid.org/0000-0002-0147-932X>

^b <https://orcid.org/0000-0002-5704-3170>

^c <https://orcid.org/0000-0002-9870-9012>

^d <https://orcid.org/0000-0002-1953-9343>

^e <https://orcid.org/0000-0001-6673-4224>

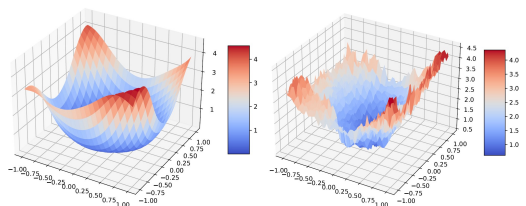


Figure 2: ResNet-18 loss landscape in single-precision (left) and low-precision number format (right).

precision decreases. To understand the effect of number format on the convergence of SGD, a careful analysis of the SGD algorithm for a predetermined precision is needed. We present both deterministic and stochastic analysis of the normalized SGD algorithm, obtaining bounds that show, explicitly, the effect of precision, i.e. number format. Such bounds can provide guidelines as to how SGD convergence is affected when constraints render performing high-precision computations impractical, and to what extent the precision can be reduced without compromising SGD convergence.

Our experiments are performed for logistic regression on MNIST dataset. They confirm that the trajectory of the loss in low-precision SGD setup has at least a limit point whose loss value is in the proximity of the minimum when the numerical errors are relatively small, see Theorem 4.1 and Theorem 4.3.

This paper is organized as follows. Section 2 presents a literature review on the low-precision training of deep learning models and also provides some common background for theoretical analysis of SGD. Section 3 discusses some preliminary notations and definitions for analysis of quasi-convex loss function and also the floating point number formats. Section 4 contains the main theoretical results. Section 5 provides some experimental results that support our theoretical results. We conclude in Section 6.

2 RELATED WORKS

Recently, deep learning models provide state-of-the-art performance in various machine learning tasks such as computer vision, speech, and natural language processing (NLP). The size of ImageNet classification models after the introduction of AlexNet size is exploded to $200\times$, and the size of language models are getting $10\times$ bigger every year. The recent trend of deep learning models shows that larger models such as transformers (Vaswani et al., 2017) and their variants such as GPT2 (Radford et al., 2019), MegatronLM (Shoeybi et al., 2019), and (Brown et al., 2020) are easier to generalize on different down-

stream tasks. Moreover, examples of large language models are included in Figure 1 (blue line) and they show an increasing trend in number of parameters over time. A similar trend also appears in vision models, specially after the advent of vision transformers ((Zhai et al., 2022);(Goyal et al., 2022)) that beat convolutional neural networks (Mahajan et al., 2018) on various tasks, see Figure 1 (black line). Although such large models have advantage in terms of accuracy, they suffer from high computational cost in their training and inference phases. Moreover, the high computational complexity of these models causes high energy consumption and memory usage which makes their training and deployment difficult and even sometimes infeasible. Thus, reducing the computational complexity of large deep learning models is crucial.

On the other hand, there has been some efforts in manually redesigning smaller models with similar accuracy as large models which often require more complicated training. In image classification small models such as MobileNet (Howard et al., 2017) have a similar accuracy as ResNet (He et al., 2016), and in language models, DistilBERT (Sanh et al., 2019) shows close performance to BERT. Meanwhile there have been some efforts in designing models automatically such as (Liu et al., 2018);(Zoph et al., 2018). Other methods include those preserving the baseline model’s architecture while modifying computations e.g. compressing large models using sparse estimation (Luo et al., 2017);(Ramakrishnan et al., 2020);(Furuya et al., 2022), or simplifying computations by running on low-precision number formats (Jacob et al., 2018);(Wu et al., 2020). Some researchers are even pushing frontiers by storing weights and reducing activation to binary (Hubara et al., 2016) or ternary numbers (Li et al., 2021).

Training large models are compute intensive using single-precision floating point. This is why hardware manufacturers such as NVIDIA, Google, Transcend, and Huawei started supporting hardware for low-precision number formats such as Bfloat, float16, and int8. Recently researchers try to map single-precision computations on lower bits, see (Zhang et al., 2020);(Zhao et al., 2021); (Ghaffari et al., 2022).

Majority of the literature on SGD assumes convex loss function. We weaken this assumption by considering quasi-convex class of loss functions that include convex functions as special case. One of the first works on quasi-convex optimization is (Kiwiel and Murty, 1996), where is proven that the gradient descent algorithm converges to a stationary point. Later, in (Kiwiel, 2001), the differentiability hypoth-

esis is removed and the convergence result is shown using quasi-subgradients. In the case of perturbed SGD, in (Hu et al., 2015) the authors are able to deal with bounded biased perturbation on the quasi-subgradient computation. In a subsequent work (Hu et al., 2016) analyzed the stochastic setting. Recently, (Zhang et al., 2022) studied the low-precision SGD for strongly convex loss functions where the authors used Langevin dynamics. In comparison, our work differs in two aspects (i) we assume quasi-convexity, (ii) our setup adds noise to the SGD and this allows for less stringent assumptions on the noise and its distribution.

3 PRELIMINARIES

We start with some preliminary notations about quasi-convexity and floating point number formats in the sequel.

3.1 Quasi-Convexity

Definition 3.1. A function $f : \mathbb{R}^d \rightarrow \mathbb{R}$ is said to be quasi-convex if $\forall a \in \mathbb{R}$, $f^{-1}[(-\infty, a)] = \{\mathbf{w} \in \mathbb{R}^d \mid f(\mathbf{w}) \in (-\infty, a)\} = \mathcal{S}_{f,a}$ is convex.

Definition 3.2. Given a quasi-convex function $f : \mathbb{R}^d \rightarrow \mathbb{R}$, the quasi-subgradient of f at $\mathbf{w} \in \mathbb{R}^d$ is defined as $\bar{\partial}^* f(\mathbf{w}) = \{g \in \mathbb{R}^d \mid \langle g, \mathbf{w}' - \mathbf{w} \rangle \leq 0, \forall \mathbf{w}' \in \mathcal{S}_{f,f(\mathbf{w})}\}$

In what follows, the optimal value and optimal set of a function f on a set Ω are respectively denoted by f^* and Ω^* , i.e. $f^* = \inf_{\mathbf{w} \in \Omega} f(\mathbf{w})$ and $\Omega^* = \operatorname{argmin}_{\mathbf{w} \in \Omega} f(\mathbf{w})$.

Definition 3.3. Let $p > 0$ and $L > 0$. $f : \mathbb{R}^d \rightarrow \mathbb{R}$ is said to satisfy the Hölder condition of order p with constant L if

$$f(\mathbf{w}) - f^* \leq L[\operatorname{dist}(\mathbf{w}, \Omega^*)]^p$$

where $\operatorname{dist}(\mathbf{w}, \mathbf{w}') = \min_{\mathbf{w}'} \|\mathbf{w} - \mathbf{w}'\|$ where $\|\cdot\|$ denotes the Euclidean norm.

The standard theory of SGD convergence relies on convex or even strict convex assumption on the loss function. Clearly quasi convex assumption is a generalization of convex assumption, i.e. all quasi convex functions are convex, but the reverse may not be true. To further motivate the quasi convex assumption we show the ResNet-56 loss-landscape projection in two and three dimensions without skip connections over the CIFAR10 dataset, see Figure 3. The convex regions and the quasi-convex regions are highlighted. The quasi-convex regions are larger than the convex regions. This means that our theory is applicable in a larger domain of the loss function.

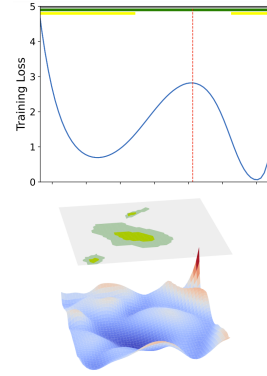


Figure 3: The quasi-convex regions (in green) are larger than the convex regions (in yellow).

3.2 Floating Points

A base $\beta \in \mathbb{N}$, with precision $t \in \mathbb{N}$, and exponent range $[e_{\min}, e_{\max}] \subset \mathbb{Z}$ define a floating point system \mathbb{F} , where an element $y \in \mathbb{F}$ can be represented as

$$y = \pm m \times \beta^{e-t}, \quad (1)$$

where $m \in \mathbb{Z}$, $0 \leq m < \beta^t$, and $e \in [e_{\min}, e_{\max}]$.

For an $x \in [\beta^{e_{\min}-t}, \beta^{e_{\max}}(1 - \beta^{-t})]$, let the float projection function be $\operatorname{fl}(x) := P_{\mathbb{F}}(x)$, then for $x, y \in \mathbb{F}$, the rounding error for basic operations $\operatorname{op} \in \{+, -, \times, /\}$, is

$$\operatorname{fl}(x \operatorname{op} y) = (x \operatorname{op} y)(1 + \delta_0), \quad (2)$$

where the error is bounded by $\delta_0 \leq \beta^{1-t}$.

When trying to compute a subgradient $g \in \partial f(\mathbf{w})$ for a $\mathbf{w} \in \mathbb{F}$ the error is bounded to

$$\operatorname{fl}(g) = g(1 + \delta_1),$$

where $|\delta_1| \leq c\delta_0$ and $c > 0$ depends on the number of operations needed for computing such subgradient. A step of subgradient descent in floating point in \mathbb{R}^d is:

$$\mathbf{w}_{k+1} = \{\mathbf{w}_k - \eta[\mathbf{g}_k(1 + \delta_{1k})]\}(1 + \delta_{2k}),$$

where we suppose $\eta \in \mathbb{F}$, $\|\delta_{1k}\| \leq c\delta_0\sqrt{d}$ and $\|\delta_{2k}\| \leq \delta_0\sqrt{d}$ where d is the dimension of δ . We can reformulate it in terms of absolute error

$$\mathbf{w}_{k+1} = \mathbf{w}_k - \eta(\mathbf{g}_k + \mathbf{r}_k) + \mathbf{s}_k,$$

and if the norm of the subgradient \mathbf{g}_k and \mathbf{w}_{k+1} is bounded, then so are $\|\mathbf{r}_k\| \leq R$ and $\|\mathbf{s}_k\| \leq S$. Note that the infinity norm of the errors are bounded

$$\|\delta_{1k}\|_{\infty} \leq c\delta_0, \quad \|\delta_{2k}\|_{\infty} \leq \delta_0,$$

so

$$R^2 \leq c\delta_0 \|\mathbf{g}_k\|, \quad S^2 \leq \delta_0 \|\mathbf{w}_k\|.$$

4 MAIN RESULTS

Although our study is mainly motivated by training deep learning models and floating point errors, they can be applied elsewhere.

4.1 Deterministic Analysis

Let $P_\Omega(\cdot)$ be the projection operator over Ω . We start with adapting and improving the results of (Hu et al., 2015) in the presence of error in the summation

Theorem 4.1. *Let $f : \mathbb{R}^d \rightarrow \mathbb{R}$ be a quasi-convex function satisfying the Hölder condition of order p and constant L . Let $\mathbf{w}_{k+1} = P_\Omega(\mathbf{w}_k - \eta \hat{\mathbf{g}}_k + \mathbf{s}_k)$ where $\Omega \subset \mathbb{R}^d$ is compact, c is the diameter of Ω , and $\hat{\mathbf{g}}_k = \frac{\mathbf{g}_k}{\|\mathbf{g}_k\|} + \mathbf{r}_k$, with $\mathbf{g}_k \in \bar{\partial}^* f(\mathbf{w}_k)$, $\|\mathbf{r}_k\| < R < 1$, $\|\mathbf{s}_k\| \leq S$. Then*

$$\liminf_{k \rightarrow \infty} f(\mathbf{w}_k) \leq f^* + L\Gamma^p(c),$$

where

$$\Gamma(c) = \frac{\eta}{2} \left[1 + \left(R + \frac{S}{\eta} \right)^2 \right] \sqrt{\left[\frac{\eta}{2} \left\{ 1 - \left(R + \frac{S}{\eta} \right)^2 \right\} + c \left(R + \frac{S}{\eta} \right) \right]}.$$

See the Appendix for the proof.

Remark: Unlike (Hu et al., 2015), decreasing η does not decrease the error bound always, so we can derive its optimal value by minimizing the bound with respect to η .

Define

$$\eta_1 = \frac{S}{\sqrt{1+R^2}}, \quad \eta_2 = \sqrt{\frac{S(c-2S)}{1-R^2}}, \quad \eta_3 = \frac{c-S}{R}$$

Corollary 4.1.1. *The optimal choice for the step size η that minimizes the error bound in Theorem 4.1 is reached in at least one of this 3 points $\{\eta_1, \eta_2, \eta_3\}$.*

The next result presents a finite iteration version of the previous result. The effect of the number of iterations K , and the starting point \mathbf{w}_0 are clearly reflected in the bound for $\min_{k < K} f(\mathbf{w}_k)$.

Theorem 4.2. *Let $f : \mathbb{R}^d \rightarrow \mathbb{R}$ be a quasi-convex function satisfying the Hölder condition of order p and constant L . Let $\mathbf{w}'_{k+1} = \mathbf{w}_k - \eta \hat{\mathbf{g}}_k$ and $\mathbf{w}_{k+1} = \mathbf{w}'_{k+1} + \mathbf{s}_k$ where $\hat{\mathbf{g}}_k = \frac{\mathbf{g}_k}{\|\mathbf{g}_k\|} + \mathbf{r}_k$, where $\mathbf{g}_k \in \bar{\partial}^* f(\mathbf{w}_k)$, $\|\mathbf{r}_k\| < R$, $\|\mathbf{s}_k\| \leq S$. Then,*

$$\min_{k < K} f(\mathbf{w}_k) \leq f^* + L \left[\Gamma(c_0) + \frac{c_0}{2\eta K} \right]^p,$$

with $c_0 = \|\mathbf{w}_0 - \mathbf{w}^*\|$.

See the Appendix for the proof.

4.2 Stochastic Analysis

Here, we present the stochastic counterpart of Theorem 4.1. The theorem requires only mild conditions on the first two moments of the errors. We start by defining the notion of stochastic quasi-subgradient.

Definition 4.1. Let \mathbf{w} and \mathbf{w}' be d -dimensional random vectors defined on the probability space $(\mathcal{W}, \mathcal{F}, \mathcal{P})$ and $f : \mathbb{R}^d \rightarrow \mathbb{R}$ be a measurable quasi-convex function. Then $\mathbf{g}(\mathbf{w})$ is called a unit noisy quasi-subgradient of f at \mathbf{w} if $\|\mathbf{g}(\mathbf{w})\| \stackrel{a.s.}{=} 1$ and $\mathcal{P}\{\mathcal{S}_{f,f(\mathbf{w})} \cap \mathcal{A}_{\mathbf{w}} \neq \emptyset\} = 0$, where $\mathcal{A}_{\mathbf{w}} = \{\mathbf{w}' : \langle \mathbf{g}(\mathbf{w}), \mathbf{w}' - \mathbf{w} \rangle > 0\}$.

Thus, inspired by results of (Hu et al., 2016), we prove the following theorem that take into account both randomness in the gradient and the computation numerical error.

Theorem 4.3. *Let $f : \mathbb{R}^d \rightarrow \mathbb{R}$ be a continuous quasi-convex function satisfying the Hölder condition of order p and constant L . Let $\mathbf{w}_{k+1} = P_\Omega[\mathbf{w}_k - \eta(\hat{\mathbf{g}}_k + \mathbf{r}_k) + \mathbf{s}_k]$ where Ω is a convex closed set, $\hat{\mathbf{g}}_k$ is a unit noisy quasi-subgradient of f at \mathbf{w}_k , \mathbf{r}_k 's are i.i.d. random vectors with $\mathbb{E}\{\mathbf{r}_k\} = \mathbf{0}$ and $\mathbb{E}\{\|\mathbf{r}_k\|^2\} = d\sigma_r^2$, and similarly \mathbf{s}_k 's are i.i.d random vectors with $\mathbb{E}\{\mathbf{s}_k\} = \mathbf{0}$ and $\mathbb{E}\{\|\mathbf{s}_k\|^2\} = d\sigma_s^2$. Further assume that $\hat{\mathbf{g}}_k$, \mathbf{s}_k , and \mathbf{r}_k are uncorrelated. Then,*

$$\liminf_{k \rightarrow \infty} f(\mathbf{w}_k) \leq f^* + L \left[\frac{\eta}{2} (1 + d\sigma_r^2) + \frac{d\sigma_s^2}{2\eta} \right]^p \quad a.s.$$

See the Appendix for the proof.

Similar to Corollary 4.1.1 one can derive the optimal step size.

Corollary 4.3.1. *The optimal step size η that minimizes the error bound in Theorem 4.3 is $\eta^* = \sqrt{\frac{d\sigma_s^2}{d\sigma_r^2 + 1}}$.*

Remark: It immediately follows the optimal step size is $\frac{\sigma_s}{\sigma_r}$ for large d .

The theorems indicate that the upper bounds increase with S and R , reflecting the effect of accumulation and multiplication errors respectively. Smaller number formats clearly lead to greater values of S and R . As for η , the step size, there is a tradeoff. To make sure that the bounds provide useful information for practical purposes, one should choose the step size such that $\frac{S}{\eta}$ ($\frac{\sigma_s}{\eta}$) is controlled. This essentially means that more accuracy is required for smaller step sizes.

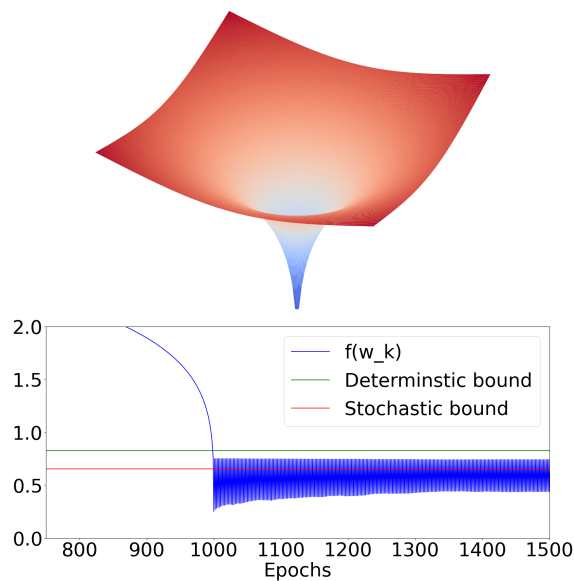


Figure 4: A two dimensional $\|\mathbf{w}\|^{0.2}$ quasi-convex function (top panel), and the SGD trace plot confirming the stochastic and deterministic bounds hold (bottom panel).

5 EXPERIMENTS

We performed two types of experiments, a simple quasi-convex function and a logistic regression on MNIST dataset.

5.1 Simple Quasi-Convex Function

To assess the bounds obtained in our theorems we start with a simple quasi-convex function that exactly satisfy the Holder’s condition. We chose $f(\mathbf{w}) = 3\|\mathbf{w}\|^{0.2}$ where $\mathbf{w} \in \mathbb{R}^{40}$. In this example, the parameters of Holder’s condition are $p = 0.2$ and $L = 3$. We added noise to the gradients and to the weight update denoted by $\|\mathbf{r}_k\|$ and $\|\mathbf{s}_k\|$ respectively. This noise has a uniform distribution $\mathbf{r}_{ki} \sim U(-B_r, B_r)$, and $s_{ki} \sim U(-B_s, B_s)$. Figure 4 shows the stochastic and deterministic bound for this experiment. Note that, the theoretical bounds holds in both stochastic and deterministic cases.

5.2 Logistic Regression

Here, we present experimental results of logistic regression on the first two principal components of MNIST dataset. For this experiment, we need to estimate the parameters of the Holder’s condition for the loss function in order to compute the bounds. To do so, the Holder’s parameters p and L are manually fitted to the loss function that is evaluated at different

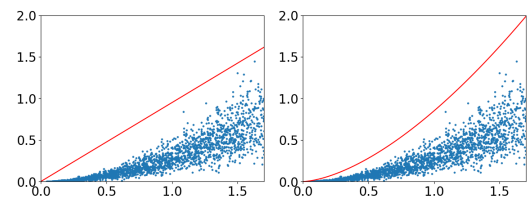


Figure 5: The Holder’s parameters p and L are manually fitted to the loss function that is evaluated at different distances from the optimal point. The left panel is a linear fit with $p = 1$ and $L = 0.95$. The right panel demonstrate the fit with $p = 1.6$ and $L = 0.85$. We used $p = 1.6$ and $L = 0.85$ for our experiments.

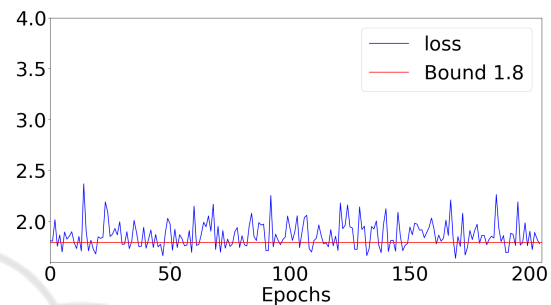


Figure 6: Logistic regression trained using single-precision SGD and a fixed learning rate.

distances from the optimal point, see Figure 5. The optimal point \mathbf{w}^* in our experiments is obtained using single-precision floating point gradient descent (GD) method and is used as a reference to compute the parameters of the bounds f^* and c .

Computation of the gradients involves inner products that are computed by multipliers and accumulators. The accumulator have numerical error relative to its mantissa size. We tested our logistic regression setup using Bfloat number format and reduced accumulator size. Also note that according to Theorem 4.3, the values of $d\sigma_s^2$ and $d\sigma_r^2$ are required to compute the bounds. Thus, in our experiments, we used empirical values of those parameters to compute the bounds. Also note that we did not plot the deterministic bounds for these experiments as they are too pessimistic.

In order to evaluate the Holder’s condition parameters, p and L , estimated as shown in Figure 5, we use a single-precision SGD to confirm if the bounds hold. Figure 6 demonstrates that the loss trajectory (blue line) has a limit point in the proximity of the optimal point of the convex loss function. Figure 7 demonstrates the loss trajectory when both weight update and gradient computations are performed using Bfloat number format. Note that Bfloat has 8 bit exponent and 7 bit mantissa and is used recently to train deep learning models. The computations are performed using 15-bit accumulator mantissa. Figure 8 shows the

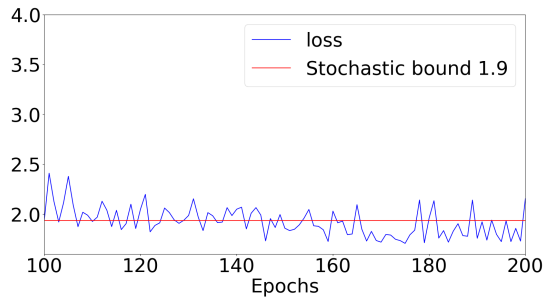


Figure 7: Logistic regression trained using Bfloat SGD with accumulator size of 15 ($\mathbf{s}_k \neq 0$ and $\mathbf{r}_k \neq 0$).

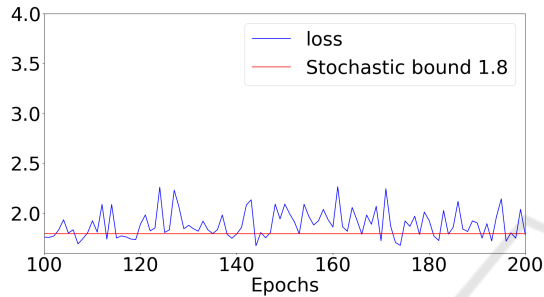


Figure 8: Logistic regression trained using Bfloat gradients with accumulator size of 15, and single-precision weight update ($\mathbf{s}_k = 0$ and $\mathbf{r}_k \neq 0$).

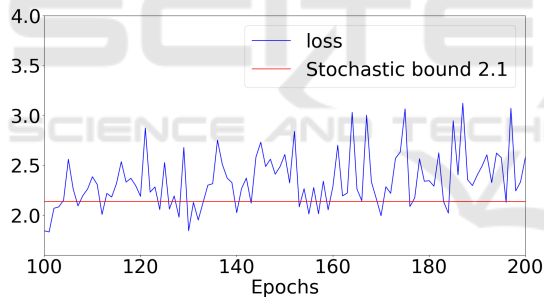


Figure 9: Logistic regression trained using Bfloat gradients with accumulator size of 10, and single-precision weight update ($\mathbf{s}_k = 0$ and $\mathbf{r}_k \neq 0$).

loss trajectory when the weight update is in single precision and only gradient computations are performed using Bfloat number format. In this experiment, the stochastic bound is numerically equal to the single-precision SGD, indicating that the precision of weight update is more important compared to the precision of the gradients.

Reducing the accumulator mantissa size has a direct effect on the convergence of SGD. Figure 9 shows that stochastic bound is increased in the case of 10-bit accumulator size. In this experiment, the loss trajectory oscillates more in the neighbourhood of the optimum point. This indicates the accumulator size plays an important role in reducing the numerical er-

rors of the low-precision SGD computations, and consequently improves the convergence of SGD.

We used the Normalized Gradient Descent (NGD) algorithm to perform the experiments with the deterministic function $f(\mathbf{w}) = \|\mathbf{w}\|^{0.2}$ presented in Section 5. The maximum number of epochs is set to 1500. Different values for C_0 , B_r , B_s and learning rates were used. The errors, which are manually added, have uniform distribution in each coordinate. Thus, the variances required in Theorem 4.3 are $\sigma_r^2 = \frac{B_r^2}{3}$ and $\sigma_s^2 = \frac{B_s^2}{3}$. For the computation of the bound in Theorem 4.1, $c = C_0$ was used.

5.3 Optimal Learning Rate

We performed experiments with fixed values for B_s , B_r , but different choices of η to acquire the optimal choice η^* given by Corollary 4.3.1. The experiment is repeated 10 times, for each tested value of η . Finally, the maximum loss function value observed across all the experiments with the same η is plotted at each epoch.

The results with $B_r = B_s = 0.1$ are shown in Figure 10 and Figure 11. The loss trajectory (blue line) observed with the value suggested by Corollary 4.3.1, $\eta = 0.0348$, is the trajectory that has the lowest level. Our theorems correctly predict that decreasing the value of η is sometimes not beneficial in terms of convergence, see Figure 11.

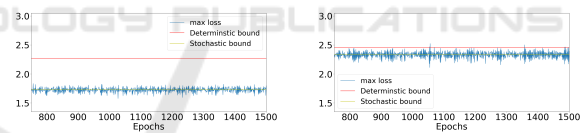


Figure 10: Results with $\eta = 0.1$ (left panel) and $\eta = 0.5$ (right panel).

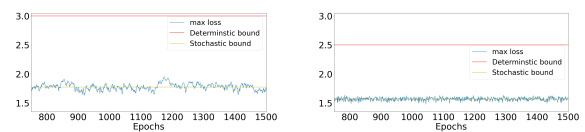


Figure 11: Results with $\eta = 0.01$ (left panel) and $\eta = 0.0348$ (right panel), decreasing the value of η leads to worse bound and worse convergence.

5.4 MNIST Image Classification

In this section the results obtained on the original MNIST dataset are reported. In contrast to the experiments in the main body of the manuscript, PCA is not used to reduce the size of the inputs.

Figure 12 demonstrates that the loss trajectory (blue line) has a limit point in the proximity of the optimal point of the convex loss function. Figure 13

shows the loss trajectory when the weight update is in single precision and only gradient computations are performed using Bfloat number format. In this experiment, the stochastic bound is numerically equal to the single-precision SGD, confirming what already observed in Figure 8.

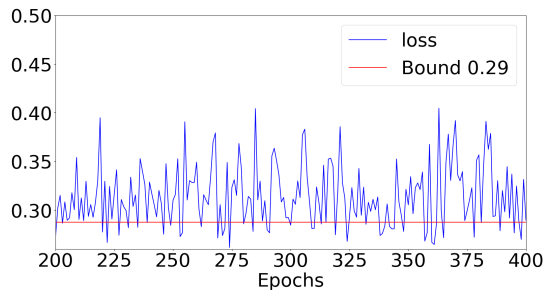


Figure 12: Logistic regression trained using single-precision SGD and a fixed learning rate.

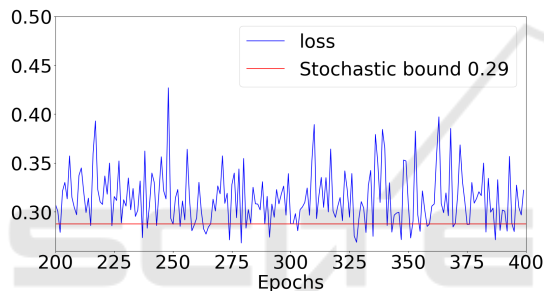


Figure 13: Logistic regression trained using Bfloat gradients with accumulator size of 50, and single-precision weight update ($s_k = 0$ and $r_k \neq 0$).

6 CONCLUSION

We have studied the convergence of low-precision floating-point SGD for quasi-convex loss functions and extended some existing deterministic and stochastic bounds for convex loss functions. In our theoretical setup, we considered numerical errors for weight update and gradient computations. We have also derived the optimal step size as a corollary of our theoretical results. Furthermore, in our experiments, the effect of numerical errors on weight update and gradient computations are demonstrated. Our experiments show that the accumulator mantissa size plays a key role in reducing the numerical error and improving the convergence of SGD. Although our experiments with logistic regression are promising, extension of the experiments for more complex models is an appealing direction as the future work.

REFERENCES

- Brown, T., Mann, B., Ryder, N., Subbiah, M., Kaplan, J. D., Dhariwal, P., Neelakantan, A., Shyam, P., Sastry, G., Askell, A., et al. (2020). Language models are few-shot learners. *Advances in neural information processing systems*, 33:1877–1901.
- Furuya, T., Suetake, K., Taniguchi, K., Kusumoto, H., Saiin, R., and Daimon, T. (2022). Spectral pruning for recurrent neural networks. In *International Conference on Artificial Intelligence and Statistics*, pages 3458–3482. PMLR.
- Ghaffari, A., Tahaei, M. S., Tayaranian, M., Asgharian, M., and Partovi Nia, V. (2022). Is integer arithmetic enough for deep learning training? *Advances in Neural Information Processing Systems*. to appear.
- Goyal, P., Duval, Q., Seessel, I., Caron, M., Singh, M., Misra, I., Sagun, L., Joulin, A., and Bojanowski, P. (2022). Vision models are more robust and fair when pretrained on uncurated images without supervision. *arXiv preprint arXiv:2202.08360*.
- He, K., Zhang, X., Ren, S., and Sun, J. (2016). Deep residual learning for image recognition. In *Proceedings of the IEEE conference on computer vision and pattern recognition*, pages 770–778.
- Howard, A. G., Zhu, M., Chen, B., Kalenichenko, D., Wang, W., Weyand, T., Andreetto, M., and Adam, H. (2017). Mobilenets: Efficient convolutional neural networks for mobile vision applications. *arXiv preprint arXiv:1704.04861*.
- Hu, Y., Yang, X., and Sim, C.-K. (2015). Inexact subgradient methods for quasi-convex optimization problems. *European Journal of Operational Research*, 240(2):315–327.
- Hu, Y., Yu, C., and Li, C. (2016). Stochastic subgradient method for quasi-convex optimization problems. *Journal of nonlinear and convex analysis*, 17:711–724.
- Hubara, I., Courbariaux, M., Soudry, D., El-Yaniv, R., and Bengio, Y. (2016). Binarized neural networks. *Advances in neural information processing systems*, 29.
- Jacob, B., Kligys, S., Chen, B., Zhu, M., Tang, M., Howard, A., Adam, H., and Kalenichenko, D. (2018). Quantization and training of neural networks for efficient integer-arithmetic-only inference. In *Proceedings of the IEEE conference on computer vision and pattern recognition*, pages 2704–2713.
- Kiwiel, K. and Murty, K. (1996). Convergence of the steepest descent method for minimizing quasiconvex functions. *Journal of Optimization Theory and Applications*, 89.
- Kiwiel, K. C. (2001). Convergence and efficiency of subgradient methods for quasiconvex minimization. *Mathematical Programming*, 90:1–25.
- Li, X., Liu, B., Yu, Y., Liu, W., Xu, C., and Partovi Nia, V. (2021). S3: Sign-sparse-shift reparametrization for effective training of low-bit shift networks. *Advances in Neural Information Processing Systems*, 34:14555–14566.

- Liu, H., Simonyan, K., and Yang, Y. (2018). Darts: Differentiable architecture search. *arXiv preprint arXiv:1806.09055*.
- Luo, J.-H., Wu, J., and Lin, W. (2017). Thinet: A filter level pruning method for deep neural network compression. In *Proceedings of the IEEE international conference on computer vision*, pages 5058–5066.
- Mahajan, D., Girshick, R., Ramanathan, V., He, K., Paluri, M., Li, Y., Bharambe, A., and Van Der Maaten, L. (2018). Exploring the limits of weakly supervised pre-training. In *Proceedings of the European conference on computer vision (ECCV)*, pages 181–196.
- Polyak, B. (1967). A general method for solving extremum problems. *Soviet Mathematics. Doklady*, 8.
- Radford, A., Wu, J., Child, R., Luan, D., Amodei, D., Sutskever, I., et al. (2019). Language models are unsupervised multitask learners. *OpenAI blog*, 1(8):9.
- Ram, S. S., Nedić, A., and Veeravalli, V. V. (2009). Incremental stochastic subgradient algorithms for convex optimization. *SIAM Journal on Optimization*, 20(2):691–717.
- Ramakrishnan, R. K., Sari, E., and Nia, V. P. (2020). Differentiable mask for pruning convolutional and recurrent networks. In *2020 17th Conference on Computer and Robot Vision (CRV)*, pages 222–229. IEEE.
- Sanh, V., Debut, L., Chaumond, J., and Wolf, T. (2019). Distilbert, a distilled version of bert: smaller, faster, cheaper and lighter. *arXiv preprint arXiv:1910.01108*.
- Schmidt, M., Roux, N., and Bach, F. (2011). Convergence rates of inexact proximal-gradient methods for convex optimization. *Advances in neural information processing systems*, 24.
- Shoeybi, M., Patwary, M., Puri, R., LeGresley, P., Casper, J., and Catanzaro, B. (2019). Megatron-lm: Training multi-billion parameter language models using model parallelism. *arXiv preprint arXiv:1909.08053*.
- Vaswani, A., Shazeer, N., Parmar, N., Uszkoreit, J., Jones, L., Gomez, A. N., Kaiser, Ł., and Polosukhin, I. (2017). Attention is all you need. *Advances in neural information processing systems*, 30.
- Wu, H., Judd, P., Zhang, X., Isaev, M., and Micikevicius, P. (2020). Integer quantization for deep learning inference: Principles and empirical evaluation. *arXiv preprint arXiv:2004.09602*.
- Zhai, X., Kolesnikov, A., Houlsby, N., and Beyer, L. (2022). Scaling vision transformers. In *Proceedings of the IEEE/CVF Conference on Computer Vision and Pattern Recognition*, pages 12104–12113.
- Zhang, R., Wilson, A. G., and De Sa, C. (2022). Low-precision stochastic gradient langevin dynamics. In *International Conference on Machine Learning*, pages 26624–26644. PMLR.
- Zhang, X., Liu, S., Zhang, R., Liu, C., Huang, D., Zhou, S., Guo, J., Guo, Q., Du, Z., Zhi, T., et al. (2020). Fixed-point back-propagation training. In *Proceedings of the IEEE/CVF Conference on Computer Vision and Pattern Recognition*, pages 2330–2338.
- Zhao, K., Huang, S., Pan, P., Li, Y., Zhang, Y., Gu, Z., and Xu, Y. (2021). Distribution adaptive int8 quantization for training cnns. In *Proceedings of the AAAI Conference on Artificial Intelligence*, volume 35, pages 3483–3491.
- Zoph, B., Vasudevan, V., Shlens, J., and Le, Q. V. (2018). Learning transferable architectures for scalable image recognition. In *Proceedings of the IEEE conference on computer vision and pattern recognition*, pages 8697–8710.